Applied Catalysis B: Environmental 142–143 (2013) 553–560

Contents lists available at SciVerse ScienceDirect

Applied Catalysis B: Environmental

journal homepage: www.elsevier.com/locate/apcatb

Photodegradation of bisphenol A by highly stable palladium-doped mesoporous graphite carbon nitride (Pd/mpg-C_3N_4) under simulated solar light irradiation

Chun Chang[a], Yu Fu[a], Meng Hu[b], Chunying Wang[a], Guoqiang Shan[a], Lingyan Zhu[a,*]

[a] Key Laboratory of Pollution Processes and Environmental Criteria, Ministry of Education, Tianjin Key Laboratory of Environmental Remediation and Pollution Control, College of Environmental Science and Engineering, Nankai University, Tianjin 300071, PR China
[b] Tourism College, Hainan University, Haikou City, Hainan 570228, PR China

ARTICLE INFO

Article history:
Received 16 January 2013
Received in revised form 4 May 2013
Accepted 22 May 2013
Available online 29 May 2013

Keywords:
Pd/mpg-C_3N_4
Bisphenol A (BPA)
Photocatalysis
Reactive oxide species (ROS)

ABSTRACT

Palladium modified mesoporous graphitic carbon nitride polymer (Pd/mpg-C_3N_4) was fabricated and used for the degradation of bisphenol A (BPA) in water. Doping Pd on the surface of mpg-C_3N_4 enhanced the light absorbance in the range of UV–vis region. Most of the embedded Pd was present as Pd^0 and could act as electron traps and facilitate the separation of photogenerated holes and electron pairs. As a result, the photocatalytic performance was improved significantly. The reaction rate constant (k_{obs}) increased with the Pd loading on the surface of mpg-C_3N_4 and the maximum was achieved with 1.50% Pd. Almost 100% of BPA (20 mg L^{-1}) was photodegraded by the solids of 0.5 g L^{-1} Pd/mpg-C_3N_4 after irradiation with simulated solar light for 360 min. The Pd/mpg-C_3N_4 exhibited very stable and high efficient photocatalytic activity to BPA in a wide range of pH 3.08–11.00. It also displayed high photocatalytic activity without photocorrosion after reuse for many times. Hydroxyl radicals, photogenerated holes, and superoxide radical species were responsible for the photodegradation while the superoxide radical species were more predominant in the Pd/mpg-C_3N_4 reaction system.

1. Introduction

Bisphenol A (BPA, 2,2-bis(4-hydroxyphenyl)propane) was first synthesized in 1891 and is used extensively in the manufacturing of consumer goods and products, such as polycarbonate food containers and utensils, food and drink packaging materials, dental sealants, protective coatings on metal equipment and so on [1,2]. BPA is one of the chemicals with high production volume, and the annual production volume is roughly over 8 billion pounds worldwide [3]. Due to its wide application, a large amount of BPA has been released into the environment, resulting ubiquitous presence of BPA in natural water [4]. Unfortunately, it was reported that BPA could cause adverse effects to human beings and wildlife, such as ovarian disease in women [5], thyroid hormone disruption [6], and carcinogenicity in adult rodents [7]. It is regarded as a representative material among endocrine disrupting chemicals (EDCs) and it becomes a great concern to control the release of BPA to natural water.

Many physical [8], chemical [9,10], and biological [11,12] remediation strategies have been proposed in recent years. Among these methods, photocatalytic degradation is attracting widespread attention due to its effective activity and low toxicity. In particular, TiO_2 has found wide application in photocatalytic degradation of organic pollutants in water body, and BPA degradation by TiO_2 had been reported [13]. However, TiO_2 could only use <5% solar energy for photodegradation due to its large bandgap energy, and this restricts its application. In recent years, many efforts have been made to explore novel photocatalysts to increase the utilization efficiency of solar energy. Wang et al. [14] reported that BPA could be degraded efficiently by Bi_2WO_6 under simulated solar light. Recently, it was reported that a metal-free polymeric photocatalyst, graphite-like carbon nitride (g-C_3N_4), displayed good visible-light-driven photocatalytic performance and could produce hydrogen or oxygen by water splitting under visible light [15,16]. Subsequently, Yan et al. [17] utilized g-C_3N_4 and boron doped g-C_3N_4 to photocatalytically degrade organic dyes. In addition, He and co-workers reported that the composites of g-C_3N_4 and vanadate displayed better photocatalytic performance than pure g-C_3N_4 [18,19]. To enhance its photocatalytic performance, mesoporous g-C_3N_4 (mpg-C_3N_4) was synthesized using silica nanoparticles as hard templates [20]. It was reported that the mpg-C_3N_4 displayed much higher H_2 evolution activity than the bulk C_3N_4

* Corresponding author at: The College of Environmental Science and Engineering, Nankai University, Weijin Road 94, Tianjin 300071, PR China. Tel.: +86 22 23500791; fax: +86 22 23508807.
E-mail address: zhuly@nankai.edu.cn (L. Zhu).

0926-3373/$ – see front matter © 2013 Elsevier B.V. All rights reserved.
http://dx.doi.org/10.1016/j.apcatb.2013.05.044

under visible light irradiation [21]. In addition, the mesoporous structure makes it as a good host for metal deposition. It was reported that embedding metal particles on the mpg-C_3N_4 constructs metal-semiconductor heterojunction and could improve the photocatalytic performance significantly [22]. However, the research about the hybrid of this metal–organic polymer is still limited.

In current study, bulk g-C_3N_4, mpg-C_3N_4 and Pd/mpg-C_3N_4 with different loading of Pd were synthesized and their photocatalytic activities to degrade BPA under simulated solar light irradiation were compared. The primary objective was to elucidate the impacts and mechanisms of Pd embedment on the photocatalytic degradation of BPA. The resultant catalysts were comprehensively characterized by means of TEM, XRD, XPS, N_2 adsorption/desorption, elemental analysis, and UV–vis DRS. The effects of Pd loading amount and initial solution pH on the photodegradation by Pd/mpg-C_3N_4 were investigated. The stability of photocatalytic performance of Pd/mpg-C_3N_4 was evaluated by conducting recycling experiments for 10 times. The possible photocatalytic mechanisms were also investigated.

2. Experimental

2.1. Materials and reagents

Ammonium bifluoride (NH_4HF_2), palladium chloride ($PdCl_2$) and potassium borohydride (KBH_4) were purchased from Tianjin Aoran Fine Chemical Industry Research Institute. Potassium hydroxide (KOH) and hydrochloric acid (HCl) were bought from chemical technology Co., Ltd., Tianjin, China. All solvents and reagents were analytical grade. Cyanamide and 12-nm SiO_2 particles (Ludox HS40) were supplied by Sigma–Aldrich Trading Co., Ltd (Shanghai). TiO_2 particles (P25, Degussa) were purchased from Degussa Corporation, Germany. BPA (purity 99.5%) was purchased from Dr. Ehrenstorfer GmbH, Augsburg, Germany.

2.2. Synthesis of bulk and mesoporous graphitic carbon nitride (g-C_3N_4 and mpg-C_3N_4)

The bulk g-C_3N_4 was synthesized by directly heating 2 g of cyanamide (CN-NH_2) in a ceramic combustion boat, which was heated in a furnace at a rate of 2.3 °C min^{-1} up to 550 °C and held for 4 h under flowing N_2. The mpg-C_3N_4 was synthesized as previously reported with a few modifications [23]. 12.0 g of cyanamide was dissolved in 30.0 g of dispersed solution with 40% of 12-nm SiO_2 particles (Ludox HS40, Aldrich) in water, which were used as a hard template. The mixture was heated at 90 °C with stirring to evaporate water. The resultant white powder was then heated at a rate of 2.3 °C min^{-1} over 4 h under flowing N_2 to reach a temperature of 550 °C, and then tempered at this temperature for an additional 4 h. The brown-yellow product was treated with ammonium bifluoride (NH_4HF_2, 4 M) for 48 h to remove the silica template. The powders were then centrifuged and washed with distilled water for four times and with ethanol twice, and dried at 70 °C under vacuum overnight.

2.3. Synthesis of Pd modified mesoporous graphitic carbon nitride (Pd/mpg-C_3N_4)

1 g of synthesized mpg-C_3N_4 was dispersed in 20 mL of ethanol in an ultrasonic bath, then a certain amount of $PdCl_2$ in hydrochloric acid solution (HCl, 0.24 mol L^{-1}) was added (detailed description is given in the Supporting Information Table S1). The mixed solution was sonicated for 15 min and then vigorously shaken for 12 h at a rate of 200 rpm using a reciprocal shaker at 60 °C. 16.92 mmol L^{-1} KBH_4 alkaline solution (KOH, 0.24 mol L^{-1}) was drop-wisely added into an equal volume of $PdCl_2$ acid solution with vigorous magnetic stirring. After the addition of KBH_4, the mixture was stirred continuously for another 30 min. The dark gray solid product was washed with deionized water four times and ethanol twice, and dried at 70 °C under vacuum for overnight.

2.4. Sorption and degradation experiments

Batch experiments were conducted in a XPA-7 photochemical reactor (Xujiang Electromechanical plant, Nanjing, China) to investigate the adsorption of BPA on the prepared materials and their photocatalytic activity to BPA. Simulated sunlight irradiation was provided by a 350 W xenon lamp (Institute of Electric Light Source, Beijing) with light intensity of 5.8 mW/cm^2, the emission spectrum of the lamp is shown in Figure S1. The reaction system was cooled by circulating water and maintained at room temperature. In quartz test tubes, a certain amount of catalysts were added followed by adding 50 ml of BPA aqueous solution at 20 mg L^{-1}. The solution was magnetically stirred during the reaction. Before irradiation, the suspension was stirred in the dark for 45 min to establish adsorption–desorption equilibrium of BPA on the catalysts. Approximately 1.5 ml of aqueous sample was withdrawn at certain time intervals and centrifuged under 6000 rpm before the analysis. Recycling tests were conducted to evaluate the stability of Pd/mpg-C_3N_4, and the detailed information is described in the Supporting Information.

2.5. Characterization and analytical methods

The prepared samples were characterized by means of TEM, XRD, XPS, N_2 adsorption/desorption, UV–vis DRS, ESR, and elemental analysis. The detailed information about the characterization methods and photoelectrochemical measurement are described in Supporting Information. The point of zero surface charge (pH_{PZC}) of Pd/mpg-C_3N_4 was measured using the pH drift method and the result is shown in Figure S2 [24]. BPA was analyzed employing a high performance liquid chromatography (HPLC), and the instrumental conditions are provided in the Supporting Information.

3. Results and discussion

3.1. Characterization of the prepared catalysts

Fig. 1 compared the TEM images of the bulk-C_3N_4, mpg-C_3N_4 and Pd/mpg-C_3N_4. As shown in Fig. 1a, the bulk-C_3N_4 displayed a typical platelet-like morphology with several crystallites. In Fig. 1b, spherical pores with a mean diameter of about 12 nm were observed in mpg-C_3N_4. These pores exactly reflected the geometric properties of the original template of SiO_2 particles, which had particle size of 12 nm. The dark spherical spots in Fig. 1c and d represented Pd incorporated in the mpg-C_3N_4. It was apparent that the Pd nanoparticles were evenly distributed and their average size was approximately 3 nm. The HRTEM image of Pd/mpg-C_3N_4 in Fig. 1d revealed that Pd was composed of a group of crystal lattices. The lattice spacing of palladium nanoparticles was estimated to be 0.228 nm, corresponding to the (1 1 1) plane of palladium.

The XRD data obtained from the bulk-C_3N_4, mpg-C_3N_4 and Pd/mpg-C_3N_4 are shown in Fig. 2a. The XRD patterns revealed the graphitic stacking of the g-C_3N_4. The strongest XRD peak at 27.4° was a characteristic peak (002) showing the interlayer stacking of aromatic systems. The interlayer distance was determined to be 0.326 nm [25], which was smaller than that of crystalline g-C_3N_4, implying a dense structure due to the localization of the electrons and stronger binding between the layers [26]. In addition, a pronounced peak at 13.1° was indexed as (1 0 0) and representative of an in-plane structural packing motif [23], estimated as 0.675 nm

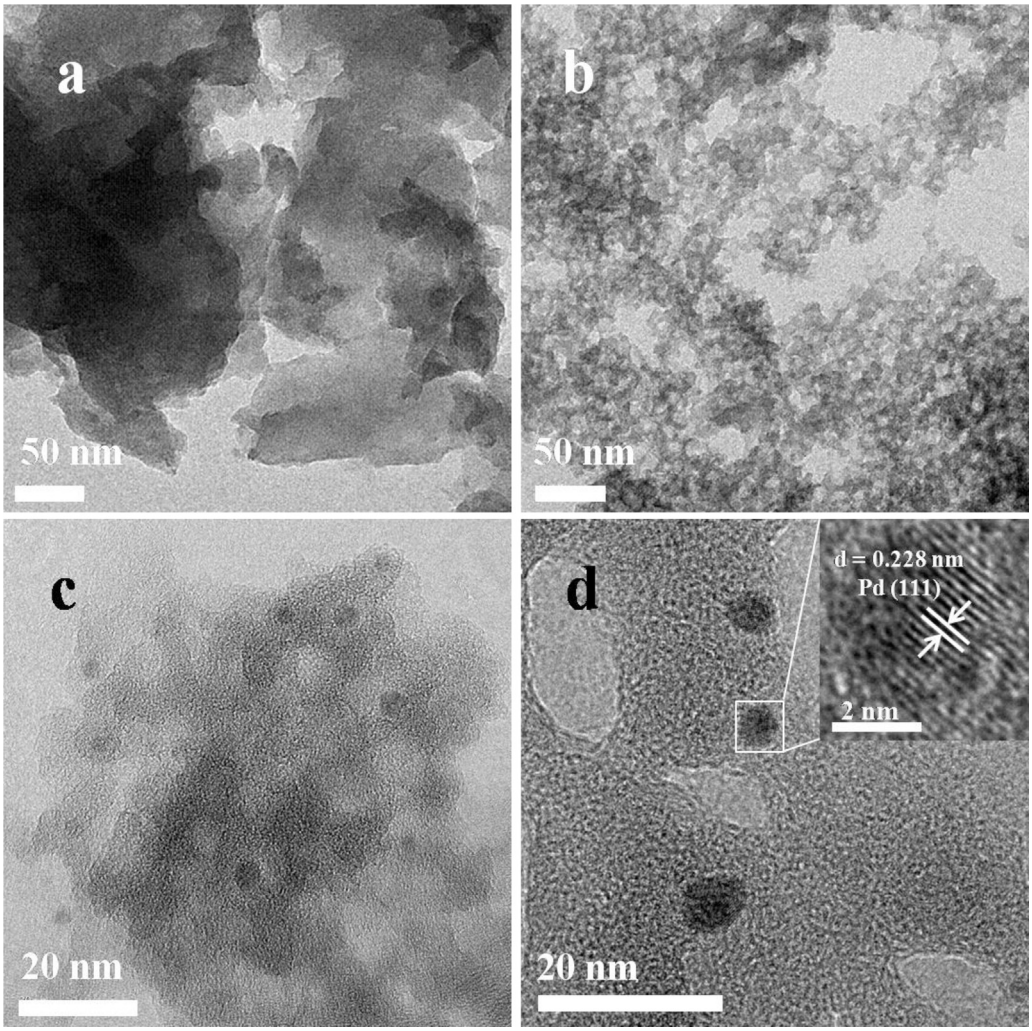

Fig. 1. The TEM images of (a) bulk-C_3N_4, (b) mpg-C_3N_4, TEM (c) and HRTEM (d) of Pd(1.5%)/mpg-C_3N_4.

(the distance of the nitride pores in the crystal). It was less than one tri-s-triazine unit (ca. 0.713 nm) and might be caused by the presence of small tilts in the structure. For mpg-C_3N_4, the (0 0 2) peak shifted slightly to higher diffraction angle as compared to the bulk materials due to the geometric confinement effect in the nano-sized pore walls. The interlayer spacing (0 0 2) was only weakly affected for those materials, but the intralayer periodicity (reflex at 13.1°, d = 0.675 nm) was significantly broadened and a decrease in the overall intensity was observed, again reflecting the effect of geometric confinement [23]. The diffraction peak observed at 40.3° in the XRD patterns of Pd/mpg-C_3N_4 with Pd loading of 4.50% could be assigned to the (1 1 1) plane of Pd nanoparticles [27].

The UV–vis diffuse reflectance spectra are depicted in Fig. 2b. The bulk g-C_3N_4 displayed absorbance in a wide range of UV to vis wavelength. As compared to the bulk material, the light absorption of mpg-C_3N_4 increased slightly. However, the embedment of Pd on mpg-C_3N_4 enhanced the absorption significantly and broadened the absorbance throughout the visible light. As the Pd loading increased, the color of the catalysts shifted from yellowish to light gray, and their light absorbance increased gradually in the range 200–700 nm. As the Pd loading content increased above 1.5%, the absorbance to the near infrared and visible light was greatly enhanced. The catalyst with 4.50% Pd displayed the strongest and most wide absorbance in the UV–vis range. The enhanced absorption might be attributed by the dark color of the Pd-embedded catalyst. On the other hand, the localized surface plasmon resonance of Pd nanoparticles deposited on mpg-C_3N_4 [28,29], which arised from the collective oscillation of the free conduction band electrons upon interaction with the incident electromagnetic radiation, might also partially contribute to the enhanced absorption. When the incident light frequency matched the plasmon oscillation frequency, light was absorbed, resulting in significant surface plasmon absorption [30,31]. The high absorption capacity might help to increase the photoactivity of mpg-C_3N_4 in the range of near infrared and visible light.

The N_2 adsorption/desorption isotherms are shown in Fig. 2c. The isotherm of the bulk-C_3N_4 was characteristic of type II according to the international union of pure and applied chemistry (IUPAC) classification, suggesting its nonporous feature. For the other two materials, the isotherms were typical of type IV with a distinct hysteresis loop observed in the range 0.65–1.00 P/P_0, indicating their mesoporous property [32,33]. This also suggested that Pd embedding does not significantly block or alter the pore structure of the mpg-C_3N_4. The BET specific surface area of the mpg-C_3N_4 was 243.20 $m^2\,g^{-1}$, which was about 54 times of the bulk g-C_3N_4 (4.49 $m^2\,g^{-1}$). In addition, the pore size distribution in Fig. 2d revealed that the pores in mpg-C_3N_4 and Pd/mpg-C_3N_4 were mainly distributed in the range 2–25 nm, corresponding to mesoporous structure. The embedment of Pd changed the properties of mpg-C_3N_4 slightly. The specific surface area of Pd/mpg-C_3N_4 was 223.42 $m^2\,g^{-1}$, slightly lower than 243.20 $m^2\,g^{-1}$ for pure mpg-C_3N_4. The average pore size decreased from 13.02 to 12.71 nm

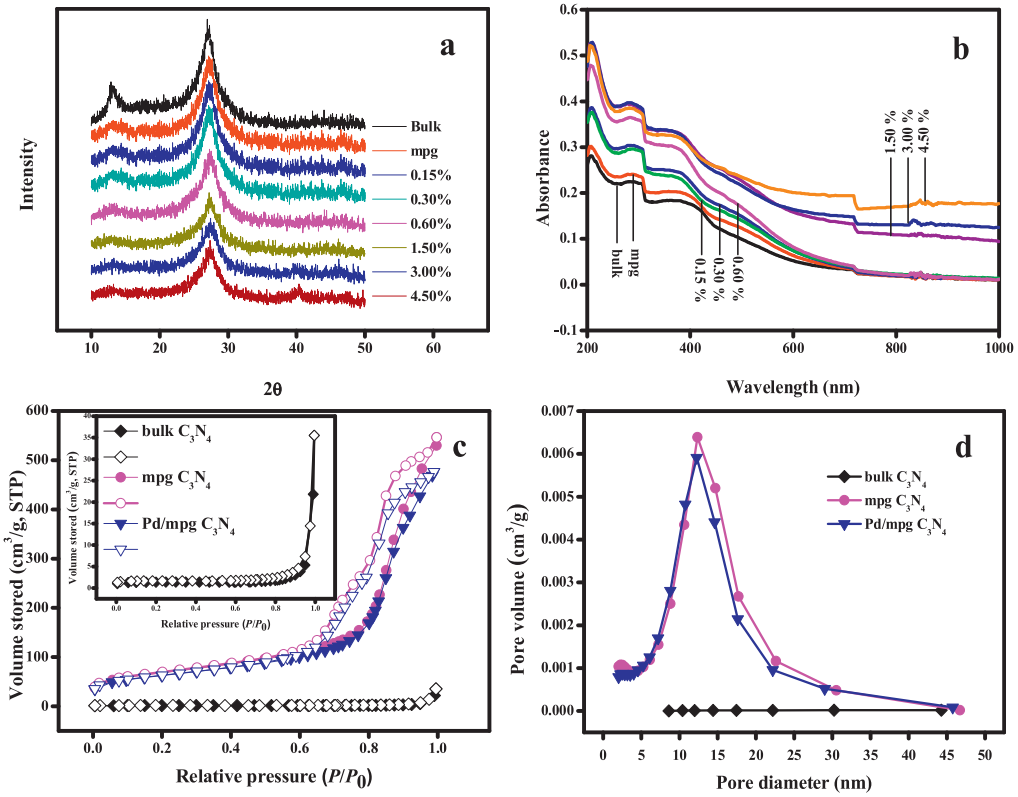

Fig. 2. (a) The XRD patterns of the prepared materials; (b) The UV–vis diffuse reflection spectra of the prepared materials; (c) The N_2 adsorption–desorption isotherms of the prepared materials. Closed symbols, adsorption; open symbols, desorption; (d) Pore size distributions of the prepared materials. *Note*: (c) and (d), Pd/mpg-C_3N_4 with Pd loading of 1.5%.

and the specific pore volume decreased from 0.80 to 0.72 $cm^3\ g^{-1}$ after embedment. These results further support that the mesopores allow the Pd nanoparticles to anchor in/on the mpg-C_3N_4 materials.

XPS were conducted to further elucidate the structure of carbon nitride and the chemical state of Pd in mpg-C_3N_4. Fig. 3b demonstrated that C1s spectrum could be fitted with four components at 284.6, 286.0, 288.1, and 293.4 eV. The component at 284.6 eV corresponded to C—C, which originated from pure graphitic carbon presumably formed during minor decomposition of the carbon nitride [34]. The peak at 286.0 eV corresponded to C═N or C≡N, which could be ascribed to defect-containing sp^2-hybridized carbon atoms present in graphitic domains [34–36]. The peak at 288.1 eV corresponded to the sp^2-hybridized carbon in N═C—N_2 coordination, which connected with three neighboring N atoms in one double and two single bonds [37]. The peak at 293.4 eV might be attributed to π-excitation [38]. In the N1s spectrum (Fig. 3c), four binding energies could be separated. The predominant peak at a binding energy of 398.6 eV might be attributed to the sp^2-hybridized nitrogen atoms in C═N—C groups [39,40]. The peak at about 400.0 eV was attributed to the tertiary nitrogen N—$(C)_3$ groups [38]. The peak at 401.1 eV was assigned to the amino function group carrying a hydrogen (C—N—H), which might be related to the structural defects and incomplete condensation in the polymerization process [39]. The additional weak peak at 404.2 eV could be ascribed to π-excitation [37]. The XPS of Pd in the modified catalyst indicated a doublet corresponding to Pd $3d_{5/2}$ and Pd $3d_{3/2}$. The Pd $3d_{5/2}$ peak consisted of two components at 335.9 and 337.0 eV, which were attributed to metallic Pd [27] and PdO [27] respectively. The relative contents of palladium species were calculated from the areas of the fitted Gaussian components in the XPS of Fig. 3d. Most of the Pd atoms (68. 5%) were present as Pd^0 on the surface of the catalyst.

The C/N ratio of the prepared materials was calculated based on the results of elemental analysis. It was in the range 0.68–0.69 (shown in Table S2), which was slightly lower than the theoretical value of C_3N_4 (0.75). This might be due to the additional small amounts of hydrogen (approximately 3.0%) to structural defects, surface termination effects by uncondensed amino functions, and adsorbed water [23].

3.2. Adsorption and degradation of BPA by Pd/mpg-C_3N_4

Figure S3 and Fig. 4a show the adsorption and photocatalytic degradation of BPA by different photocatalysts (P25 TiO_2, bulk g-C_3N_4, mpg-C_3N_4 and Pd/mpg-C_3N_4 with Pd loading of 1.5%). The BPA solution was mixed with the catalysts in dark for 180 min, and the results showed that the removal of BPA by adsorption on the catalysts was less than 4.0% (Figure S3). As a comparison, BPA photolysis without any photocatalyst was also investigated. The results demonstrated that BPA was hardly degraded in the absence of photocatalyst under simulated solar light (Fig. 4a). It was obvious that bulk g-C_3N_4 and P25 TiO_2 exhibited very weak photocatalytic activity and only 6.0 and 6.7% of BPA was degraded after irradiation for 180 min, respectively. The degradation of BPA increased to 52.1% when mpg-C_3N_4 was used as photocatalyst. The specific surface area of mpg-C_3N_4 was 54 times of the bulk g-C_3N_4. Thus mpg-C_3N_4 could provide more catalytic active sites for the reactions. In addition, the defects in mpg-C_3N_4 could induce electron relocalization in the graphitic layer and promote the catalytic activity [23]. Moreover, mesopores allowed light waves to penetrate deep inside the photocatalyst and lead to high mobility of charges, resulting in a promoted photocatalytic activity [14,41]. As compared to these catalysts, the Pd/mpg-C_3N_4 exhibited the highest photocatalytic activity with 93.9% of BPA removal from the

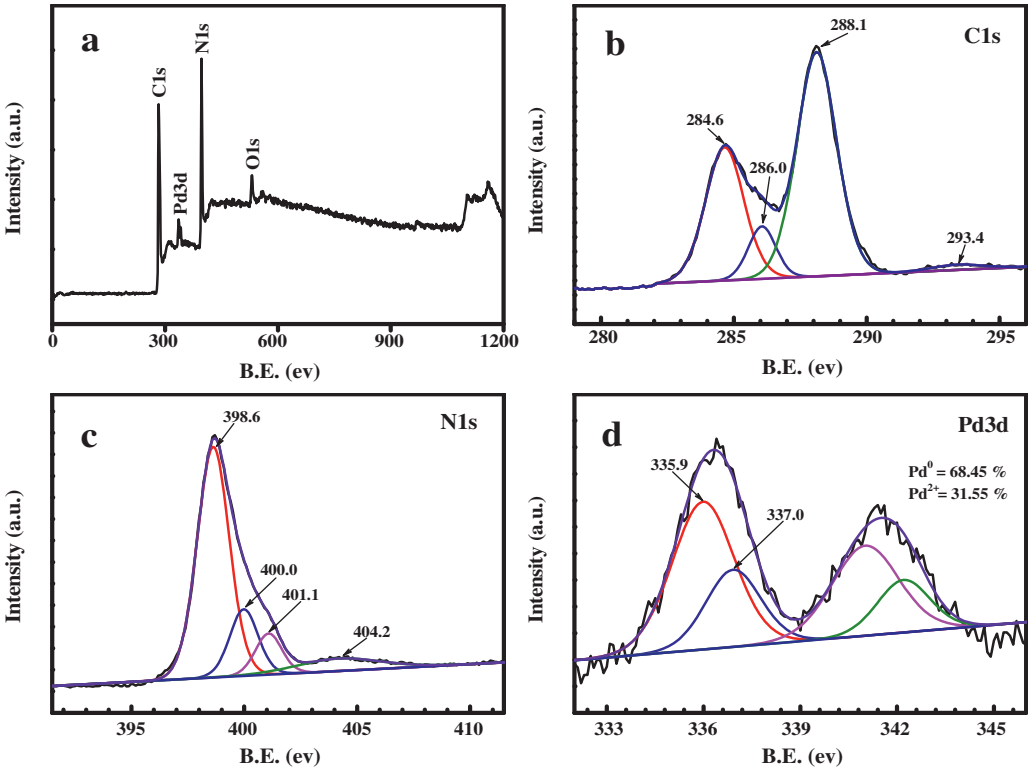

Fig. 3. The XPS spectrum of the Pd(4.5%)/mpg-C_3N_4 composite. (a) Full scan; (b) C1s; (c) N1s; and (d) Pd3d.

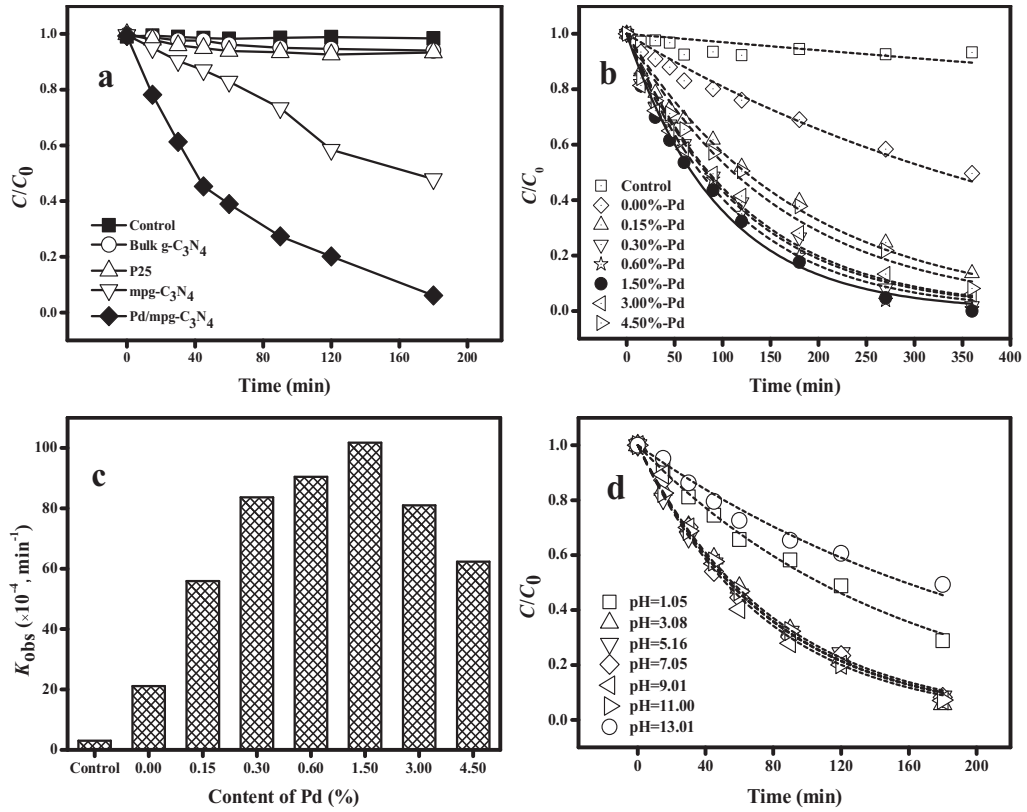

Fig. 4. (a) The degradation rates of the prepared catalysts. (Photocatalyst, 1.0 g L^{-1}; pH, 6.28; irradiation time, 180 min). (b) and (c) The photocatalytic efficiency of BPA with mpg-C_3N_4 and of Pd/mpg-C_3N_4 with different Pd contents. (Photocatalyst, 0.5 g L^{-1}; pH, 6.28; irradiation time, 360 min). (d) Influence of the initial pH on the photocatalytic reaction of BPA. (Pd/mpg-C_3N_4 with Pd loading of 1.5%, 1.0 g L^{-1}; irradiation time, 180 min). Initial concentration of BPA, 20 mg L^{-1} aqueous solution (containing 1% methanol, v/v).

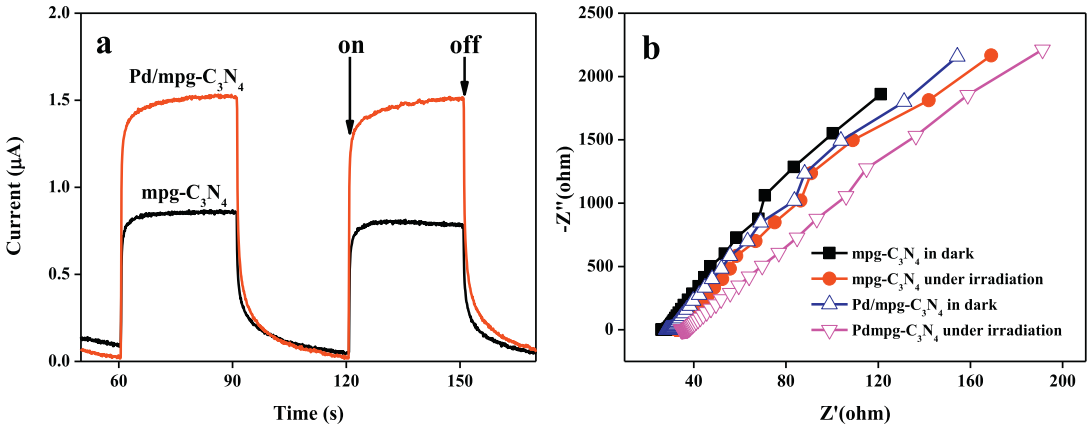

Fig. 5. Photoresponses (a) and EIS Nyquist plots (b) of the mpg-C_3N_4 and 1.5% Pd/mpg-C_3N_4 photocatalyst.

solution within 180 min irradiation. Since metal Pd particles could act to trap photo-induced electrons, the recombination of electron–hole pairs was retarded, and thereby, the photocatalytic activity was improved. In addition, PdO also has strong electron affinity and can be readily reduced by capturing the photogenerated electrons ($Pd^{2+} + 2e = Pd$). The electron–hole pairs were efficiently separated and interfacial charge transfer was greatly promoted, resulting in enhanced photoactivity of mpg-C_3N_4 [31,42].

Photoeletrochemical performance could be used to evaluate the efficiency of photogenerated charge interface separation for photocatalytic performance [25]. The photoresponses of ITO/mpg-C_3N_4 and 1.5% ITO/Pd/mpg-C_3N_4 electrodes in on-off cycles under visible light irradiation were examined and the results are shown in Fig. 5a. The photocurrent intensity generated by Pd/mpg-C_3N_4 electrode was twice of that induced by mpg-C_3N_4, suggesting more efficient separation of photogenerated electron–hole pairs in Pd/mpg-C_3N_4. The interface charge separation efficiency was also investigated by EIS. A smaller arc radium in the EIS Nyquist plot implies an effective separation of the photogenerated electron–hole pairs [43]. Fig. 5b illustrates that the impedance arc radii of mpg-C_3N_4 and Pd/mpg-C_3N_4 in dark were larger than that under visible light irradiation, implying that there were a few electrons across the mpg-C_3N_4 or Pd/mpg-C_3N_4 electrolyte interface without irradiation. The arc radium of Pd/mpg-C_3N_4 was smaller than that of mpg-C_3N_4 under simulated solar light irradiation further supports that the photogenerated electron–hole pairs were more effectively separated in the system with Pd/mpg-C_3N_4 and there was a more efficient interfacial charge transfer between the electron donor and electron acceptor.

3.3. Effect of Pd loading on degradation efficiency

In the control test without catalysts, only 6.70% of BPA was degraded under irradiation of simulated solar light for 6 h, suggesting that the photolysis of BPA by direct light irradiation is very weak. The following pseudo first-order reaction kinetic model might be used to describe the degradation reaction of BPA:

$$\frac{C_{BPA,t}}{C_{BPA,0}} = e^{-k_{obs}t}$$

where $C_{BPA,t}$ was the concentration of BPA in aqueous phase ($mg\,L^{-1}$), $C_{BPA,0}$ was the initial concentration of BPA ($mg\,L^{-1}$), k_{obs} was the pseudo first-order rate constant (min^{-1}) and t was the reaction time (min). The pseudo first-order reaction kinetic model fitted the experimental data very well with regression coefficient $R^2 > 0.9669$ in all cases. A linear fitting of $\ln(C/C_0)$ and t would give the reaction rate constant k_{obs}. The reaction kinetics and k_{obs}s of the reactions with Pd/mpg-C_3N_4 containing different loading of Pd were shown in Fig. 4b and 4c. The degradation efficiency in 6 h increased gradually from 50.40 to 100% as Pd content increased from 0 to 1.5% and then slightly decreased to 91.91% as the content further increased to 4.5%. The maximum k_{obs} was achieved with Pd loading of 1.5%, and it was approximately 5 times of the reaction using pure mpg-C_3N_4 under the same conditions. Since Pd and PdO nanoparticles could act as electron traps and facilitate the separation of photogenerated electron–hole pairs, more doped Pd would promote interfacial electron transfer efficiency and enhance the photodegradation. Similar effect was also reported for Ag-loaded Bi_2WO_6 [31] and Ag–TiO_2 hybrid catalysts [44]. However, as the loading of Pd further increases, they could behave as recombinant centers. It was widely reported that over abundance of metal or non-metal impurities would become the recombination centers of electrons and holes, leading to lower photocatalytic efficiency [31,42]. In addition, Pd nanoparticles could aggregate as the loading amount increases, also inhibiting the photodegradation [45].

3.4. Effect of initial pH on photocatalytic activities of Pd/mpg-C_3N_4

The initial pH of the aqueous solution might affect the surface charge of the amphoteric semiconductor photocatalyst and the ionization of BPA in the solution. Therefore, the effect of initial pH on the BPA photodegradation efficiency was investigated in the range 1.05–13.01. Fig. 4d shows the reaction kinetics under different pH. The reaction rate constant k_{obs} distinctly increased as the pH increased from 1.05 to 3.08. In a wide pH range 3.08–11.00, the degradation efficiency remained quite constant. However, the degradation efficiency decreased greatly as the pH further increased from 11.00 to 13.01. It was reported that the most active system in mpg-C_3N_4 was the incompletely condensed, N-bridged poly(tri-s-triazine) polymer. The nitrogen functionalities on the surface might act as strong Lewis base sites. It was suggested that phenol molecules interact with the surface via special O—H···N or O—H···π interactions [27]. At very low pH (<3.08), large amounts of H^+ were adsorbed on the surface of mpg-C_3N_4 by interaction with N atoms, competing with BPA molecules for the active sites. Thus, the catalyst displayed very low photocatalytic efficiency to BPA at low pH. The zero point charge of the catalyst was determined to be about 2.1. As the pH was higher than 2.1, the catalyst was negatively charged and favors the interaction of BPA with the catalyst surface via O—H···N or O—H···π. Therefore, the catalyst displayed very stable and effective degradation efficiency to BPA at pH 3.08–11.00. However, as the pH was higher than the acid dissociation constant

pK_a of BPA (9.6–11.3) [46], bisphenolate anion (—O—$C_{15}H_{14}$—O—) might be formed due to deprotonation. The interaction between BPA and the catalyst decreased, resulting lower photodegradation efficiency at high pH > 11.00. Unlike the photocatalyst of sulfide and metallic oxide semiconductor, the photocatalytic efficiency of which was highly dependent on pH, the Pd/mpg-C_3N_4 demonstrated very stable and high photocatalytic efficiency to BPA in a rather wide pH range. This was very significant for its real application in the treatment of industrial wastewater that usually had a wide range of pH values.

3.5. Stability of photocatalytic performance of Pd/mpg-C_3N_4

The reuse of the Pd/mpg-C_3N_4 for photocatalytic degradation of BPA under simulated solar light was investigated to evaluate the optical stability of the catalyst and the results are shown in Figure S4. The Pd/mpg-C_3N_4 did not exhibit significant loss of photocatalytic activity after three recycling runs, and still maintained about 84% after six recycling runs and about 72% after ten recycling runs respectively. The results indicated that Pd/mpg-C_3N_4 keeps its photocatalytic activity without distinct photocorrosion during the oxidation of BPA. The slight decreased in degradation efficiency over several runs could be attributed to the mass loss of catalyst during the washing procedure.

3.6. Photocatalytic mechanism of Pd/mpg-C_3N_4 on BPA

The active species responsible for the oxidative reaction which were formed during the light irradiation progress were monitored by DMPO spin-trapped ESR spectroscopy, and the results are shown in the Figure S5. In the two photocatalysis systems with P25 and Pd/mpg-C_3N_4, exclusively 1:2:2:1 quartet characteristic peaks for DMPO-•OH adducts were observed in the ESR spectra, indicating that the •OH radicals were formed [17,47,48]. The •OH might be generated by direct hole oxidation [49] or photogenerated electron-induced multistep reduction of O_2 [17]. For Pd/mpg-C_3N_4, the standard redox potentials of the top valance band (1.92 ± 0.03 V vs. NHE) of mpg-C_3N_4 [50] and Pd^{IV}/Pd^{II} (1.47 V vs. NHE) [51] were smaller than that of •OH/OH— (1.99 V vs. NHE) [52] and •OH/H_2O (2.27 V vs. NHE) [16], suggesting that the photogenerated holes and Pd^{IV} on the surface of mpg-C_3N_4 were incapable of directly oxidizing adsorbed OH— groups to •OH. Therefore, the •OH formed in the Pd/mpg-C_3N_4 photocatalytic reaction system was mainly from the reduction of O_2. The difference in the photocatalytic reaction rate between P25 and Pd/mpg-C_3N_4 might be due to the fact that some other reactive oxygen species (ROSs), such as superoxide radical (•O_2 or HOO•) and hydrogen peroxide (H_2O_2), were formed during the photocatalytic reaction via light irradiation.

To further illustrate the contributory roles of these ROSs in the photodegradation process, methanol (CH_3OH) [53,54], potassium iodide (KI) [53,55], and benzoquinone (BQ) [55,56] were added in the reaction solution as the scavenger of •OH, trapping reagent of photogenerated holes, and superoxide radical respectively. Fig. 6a showed that the photodegradation efficiency of BPA by P25 TiO_2 declined significantly with the increase of CH_3OH in the solution. This suggested the pivotal role of •OH as an important species for the photocatalytic removal of BPA by P25 TiO_2 [55]. However, the photodegradation of BPA in the reaction system of Pd/mpg-C_3N_4 was slightly depressed with the addition of identical amount of CH_3OH, denoting that •OH was not the major oxidative species in photodegradation of BPA by Pd/mpg-C_3N_4. As shown in Fig. 6b, the photodegradation of BPA by P25 TiO_2 was enhanced with the increase of KI amount added in the solution, implying that scavenging h^+ might improve the electron–hole separation and increase the amount of free electrons, generating more •OH radicals. However, the photodegradation of BPA was greatly suppressed when

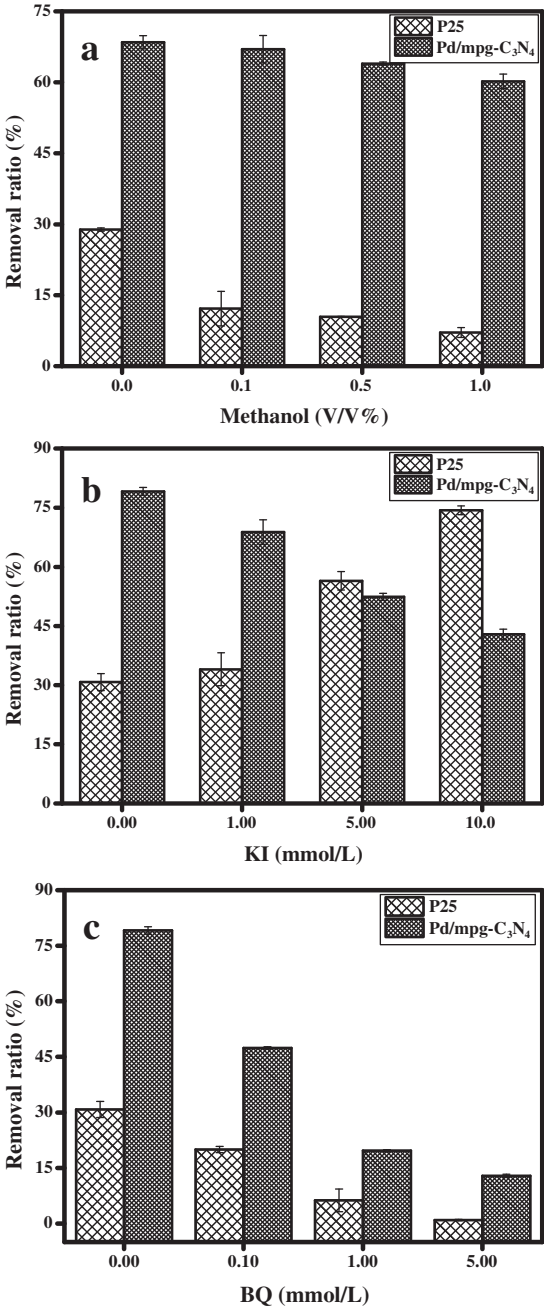

Fig. 6. Effects of methanol (a), KI (b), and BQ (c) on the photodegradation of BPA by Pd(1.5%)/mpg-C_3N_4 and P25 under simulated solar light irradiation. Irradiation time: Pd/mpg-C_3N_4 ((a), 50 min; (b) and (c) 60 min), P25 ((a), (b), and (c) 90 min).

Pd/mpg-C_3N_4 was used as photocatalyst, which strongly implied that the photogenerated holes were crucial to the photocatalytic reaction [17]. When BQ was added into the two reaction systems, the photocatalytic reactions were all significantly inhibited, as shown in Fig. 6c. The removal efficiency of BPA gradually decreased with increasing BQ concentration. Moreover, the inhibitory effect was more obvious with the addition of BQ compared to other scavengers. This result reflected that superoxide radicals might be a predominant active species responsible for the photocatalytic reaction. Pd^0 (or PdO), as a trap of the photogenerated electrons, could efficiently pass electrons to O_2 in the solution to produce superoxide radicals ($O_2^{\bullet -}$), which might react with H^+ to form $HO_2^{\bullet -}$. It is reported that superoxide radicals, such as $O_2^{\bullet -}$ and $HO_2^{\bullet -}$, were

very active radicals for the ring cleavage of aromatic compounds [55].

4. Conclusions

Doping Pd on the surface of mpg-C_3N_4 enhanced the light absorbance in the UV–vis range and photocatalytic performance significantly. The reaction rate constant (k_{obs}) increased with the Pd loading on the surface of mpg-C_3N_4 and the maximum was achieved with 1.50% Pd. Almost 100% of BPA (20 mg L^{-1}) was photodegraded by the solids of 0.5 g L^{-1} Pd/mpg-C_3N_4 after irradiation with simulated solar light for 360 min. The composites displayed a good potential in real application due to the stability in a wide range of pH (3.08–11.00) and resistance to photocorrosion after reuse for many times.

Supplementary data

The detailed information about the characterization methods, recycling test and analytical methods; the amount of $PdCl_2$ and KBH_4used for the synthesis of Pd/mpg-C_3N_4; the elemental compositions of the prepared materials; the results of point of zero surface charge (pH_{PZC}) of Pd/mpg-C_3N_4 using the pH drift method; the adsorption of the prepared catalysts; the results of the recycling tests of Pd/mpg-C_3N_4; and ESR spectra for the DMPO-containing aqueous suspensions of P25 and Pd/mpg-C_3N_4.

Acknowledgements

The authors gratefully acknowledge the financial support of Ministry of Education (Grant 708020); Tianjin Municipal Science and Technology Commission (10SYSYJC27200), Ministry of Science and Technology (2012ZX07529-003), Ministry of Environmental Protection (201009026) and the Fundamental Research Funds for the Central Universities.

Appendix A. Supplementary data

Supplementary data associated with this article can be found, in the online version, at http://dx.doi.org/10.1016/j.apcatb.2013.05.044.

References

[1] J.G. Hengstler, H. Foth, T. Gebel, P.J. Kramer, W. Lilienblum, H. Schweinfurth, W. Volkel, K.M. Wollin, U. Gundert-Remy, Critical Reviews in Toxicology 41 (2011) 263–291.
[2] Y.B. Wetherill, B.T. Akingbemi, J. Kanno, J.A. McLachlan, A. Nadal, C. Sonnenscheing, C.S. Watson, R.T. Zoeller, S.M. Belcher, Reproductive Toxicology 24 (2007) 178–198.
[3] L.N. Vandenberg, I. Chahoud, J.J. Heindel, V. Padmanabhan, F.J.R. Paumgartten, G. Schoenfelder, Environmental Health Perspectives 118 (2010) 1055–1070.
[4] D.P. Subagio, M. Srinivasan, M. Lim, T.T. Lim, Applied Catalysis B 95 (2010) 414–422.
[5] T. Takeuchi, O. Tsutsumi, Y. Ikezuki, Y. Takai, Y. Taketani, Endocrine Journal 51 (2004) 165–169.
[6] R.T. Zoeller, R. Bansal, C. Parris, Endocrinology 146 (2005) 607–612.
[7] R.A. Keri, S.M. Ho, P.A. Hunt, K.E. Knudsen, A.M. Soto, G.S. Prins, Reproductive Toxicology 24 (2007) 240–252.
[8] B. Pan, D.H. Lin, H. Mashayekhi, B.S. Xing, Environmental Science and Technology 42 (2008) 5480–5485.
[9] E.M. Rodriguez, G. Fernandez, N. Klamerth, M.I. Maldonado, P.M. Alvarez, S. Malato, Applied Catalysis B 95 (2010) 228–237.
[10] Y.H. Cui, X.Y. Li, G.H. Chen, Water Research 43 (2009) 1968–1976.
[11] T. Hirooka, H. Nagase, K. Uchida, Y. Hiroshige, Y. Ehara, J.-i. Nishikawa, T. Nishihara, K. Miyamoto, Z. Hirata, Environmental Toxicology and Chemistry 24 (2005) 1896–1901.
[12] Y.T. Xie, H.B. Li, L. Wang, Q.A. Liu, Y. Shi, H.Y. Zheng, M. Zhang, Y.T. Wu, B. Lu, Water Research 45 (2011) 1189–1198.
[13] Y. Ohko, I. Ando, C. Niwa, T. Tatsuma, T. Yamamura, T. Nakashima, Y. Kubota, A. Fujishima, Environmental Science and Technology 35 (2001) 2365–2368.
[14] C.Y. Wang, H. Zhang, F. Li, L.Y. Zhu, Environmental Science and Technology 44 (2010) 6843–6848.
[15] X.C. Wang, K. Maeda, A. Thomas, K. Takanabe, G. Xin, J.M. Carlsson, K. Domen, M. Antonietti, Nature Materials 8 (2009) 76–80.
[16] Y. Cui, J. Huang, X. Fu, X. Wang, Catalysis Science & Technology 2 (2012) 1396–1402.
[17] S.C. Yan, Z.S. Li, Z.G. Zou, Langmuir 26 (2010) 3894–3901.
[18] T. Li, L. Zhao, Y. He, J. Cai, M. Luo, J. Lin, Applied Catalysis B 129 (2013) 255–263.
[19] Y. He, J. Cai, T. Li, Y. Wu, Y. Yi, M. Luo, L. Zhao, Industrial and Engineering Chemistry Research 51 (2012) 14729–14737.
[20] M. Groenewolt, M. Antonietti, Advanced Materials 17 (2005) 1789–1792.
[21] X.C. Wang, K. Maeda, X.F. Chen, K. Takanabe, K. Domen, Y.D. Hou, X.Z. Fu, M. Antonietti, Journal of the American Chemical Society 131 (2009) 1680–1681.
[22] Y. Di, X.C. Wang, A. Thomas, M. Antonietti, Chemcatchem 2 (2010) 834–838.
[23] F. Goettmann, A. Fischer, M. Antonietti, A. Thomas, Angewandte Chemie International Edition 45 (2006) 4467–4471.
[24] B. Xiao, K.M. Thomas, Langmuir 21 (2005) 3892–3902.
[25] X.C. Wang, X.F. Chen, A. Thomas, X.Z. Fu, M. Antonietti, Advanced Materials 21 (2009) 1609–1612.
[26] S.C. Yan, Z.S. Li, Z.G. Zou, Langmuir 25 (2009) 10397–10401.
[27] Y. Wang, J. Yao, H.R. Li, D.S. Su, M. Antonietti, Journal of the American Chemical Society 133 (2011) 2362–2365.
[28] C. Langhammer, Z. Yuan, I. Zorić, B. Kasemo, Nano Letters 6 (2006) 833–838.
[29] Y. Xiong, B. Wiley, J. Chen, Z.-Y. Li, Y. Yin, Y. Xia, Angewandte Chemie International Edition 44 (2005) 7913–7917.
[30] P. Wang, B. Huang, X. Zhang, X. Qin, H. Jin, Y. Dai, Z. Wang, J. Wei, J. Zhan, S. Wang, J. Wang, M.-H. Whangbo, Chemistry: A European Journal 15 (2009) 1821–1824.
[31] J. Ren, W.Z. Wang, S.M. Sun, L. Zhang, J. Chang, Applied Catalysis B 92 (2009) 50–55.
[32] Y. Huang, Z.H. Ai, W.K. Ho, M.J. Chen, S. Lee, Journal of Physical Chemistry C 114 (2010) 6342–6349.
[33] M. Ge, Y.F. Li, L. Liu, Z. Zhou, W. Chen, Journal of Physical Chemistry C 115 (2011) 5220–5225.
[34] V.N. Khabashesku, J.L. Zimmerman, J.L. Margrave, Chemistry of Materials 12 (2000) 3264–3270.
[35] W. Lei, D. Portehault, R. Dimova, M. Antoniettit, Journal of the American Chemical Society 133 (2011) 7121–7127.
[36] Q.J. Xiang, J.G. Yu, M. Jaroniec, Journal of Physical Chemistry C 115 (2011) 7355–7363.
[37] Q.X. Guo, Y. Xie, X.J. Wang, S.Y. Zhang, T. Hou, S.C. Lv, Chemical Communications (2004) 26–27.
[38] A.P. Dementjev, A. de Graaf, M.C.M. van de Sanden, K.I. Maslakov, A.V. Naumkin, A.A. Serov, Diamond and Related Materials 9 (2000) 1904–1907.
[39] Z.X. Ding, X.F. Chen, M. Antonietti, X.C. Wang, Chemsuschem 4 (2011) 274–281.
[40] Y.G. Li, J.A. Zhang, Q.S. Wang, Y.X. Jin, D.H. Huang, Q.L. Cui, G.T. Zou, Journal of Physical Chemistry B 114 (2010) 9429–9434.
[41] C. Guo, M. Ge, L. Liu, G. Gao, Y. Feng, Y. Wang, Environmental Science and Technology 44 (2010) 419–425.
[42] C. Young, T.M. Lim, K. Chiang, J. Scott, R. Amal, Applied Catalysis B 78 (2008) 1–10.
[43] F.X. Xiao, F.C. Wang, X.Z. Fu, Y. Zheng, Journal of Materials Chemistry 22 (2012) 2868–2877.
[44] K. Awazu, M. Fujimaki, C. Rockstuhl, J. Tominaga, H. Murakami, Y. Ohki, N. Yoshida, T. Watanabe, Journal of the American Chemical Society 130 (2008) 1676–1680.
[45] P. Fu, P. Zhang, J. Li, Applied Catalysis B 105 (2011) 220–228.
[46] C.A. Staples, P.B. Dome, G.M. Klecka, S.T. Oblock, L.R. Harris, Chemosphere 36 (1998) 2149–2173.
[47] C.Y. Wang, L.Y. Zhu, C. Song, G.Q. Shan, P. Chen, Applied Catalysis B 105 (2011) 229–236.
[48] L.S. Zhang, K.H. Wong, H.Y. Yip, C. Hu, J.C. Yu, C.Y. Chan, P.K. Wong, Environmental Science and Technology 44 (2010) 1392–1398.
[49] S.H. Yoon, J.H. Lee, Environmental Science and Technology 39 (2005) 9695–9701.
[50] K. Takanabe, K. Kamata, X.C. Wang, M. Antonietti, J. Kubota, K. Domen, Physical Chemistry Chemical Physics 12 (2010) 13020–13025.
[51] G.-H. Moon, Y. Park, W. Kim, W. Choi, Carbon 49 (2011) 3454–3462.
[52] H.B. Fu, S.C. Zhang, T.G. Xu, Y.F. Zhu, J.M. Chen, Environmental Science and Technology 42 (2008) 2085–2091.
[53] C. Wang, L. Zhu, M. Wei, P. Chen, G. Shan, Water Research 46 (2012) 845–853.
[54] R. Hazime, C. Ferronato, L. Fine, A. Salvador, F. Jaber, J.M. Chovelon, Applied Catalysis B 126 (2012) 90–99.
[55] J.W. Ng, X.P. Wang, D.D. Sun, Applied Catalysis B 110 (2011) 260–272.
[56] X.P. Wang, T.T. Lim, Applied Catalysis A 399 (2011) 233–241.